Three-Dimensional FDTD Analysis of a Pulsed Microwave Confocal System for Breast Cancer Detection: Design of an Antenna-Array Element

Susan C. Hagness, *Member, IEEE,* Allen Taflove, *Fellow, IEEE,* and Jack E. Bridges, *Life Fellow, IEEE*

***Abstract*—We are investigating a new ultrawide-band (UWB) microwave radar technology to detect and image early-stage malignant breast tumors that are often invisible to X rays. In this paper, we present the methodology and initial results of three-dimensional (3-D) finite-difference time-domain (FDTD) simulations. The discussion concentrates on the design of a single resistively loaded bowtie antenna element of a proposed confocal sensor array. We present the reflection, radiation, and scattering properties of the electromagnetic pulse radiated by the antenna element within a homogeneous, layered half-space model of the human breast and the polarization and frequency-response characteristics of generic tumor shapes. We conclude that the dynamic range of a sensor array comprised of such elements in conjunction with existing microwave equipment is adequate to detect small cancerous tumors usually missed by X-ray mammography.**

***Index Terms*—Antenna array, cancer, FDTD methods.**

I. Introduction

A potentially important strategy for reducing breast cancer mortality is the detection of early-stage tumors [1]. X-ray mammography is currently the most effective screening modality for detecting clinically occult breast cancers. However, approximately 10–30% of breast cancers are missed by mammography [2], [3]. The significant number of false negatives may be attributed to the limitations of mammography in: 1) assessing dense glandular tissue and regions located close to the chest wall or underarm and 2) imaging very early-stage tumors that do not yet exhibit microcalcifications. Another concern is the high rate of false positives in screening mammograms [3], [4]. These statistics indicate a critical need for complementary modalities with high sensitivity and specificity for early detection through low-cost screening. Ultrasound and contrast-enhanced MRI are effective in the diagnostic evaluation of mammographically detected breast lesions. However, these modalities are either not sensitive/specific enough or are too costly for mass screening purposes [5]–[8].

We are investigating an ultrawide-band (UWB) microwave radar technology to detect early-stage breast cancer. The cardinal feature of this technology is the differential microwave backscatter response from tissues based on their water content, a tissue-radiation interaction mechanism that is distinct from density-based attenuation of X rays. According to the literature, the differing water content of normal and malignant breast tissues results in an order-of-magnitude dielectric-property contrast at microwave frequencies. The system under consideration has the potential to detect very small noncalcified cancers, including those in radiographically dense breasts and in regions near the chest wall or underarm. Furthermore, this approach avoids exposure to ionizing radiation, is noninvasive, and does not require breast compression. The radio-frequency exposure is well within the safety limits set by ANSI/IEEE [9]. The safety, comfort, ease-of-use, and low-cost features of the new approach should permit frequent screening of the general public and regular monitoring of patients with detected abnormalities. Augmenting X-ray mammography in this manner could help to reduce the number of false negatives and false positives.

The new modality is based on the principle of the confocal optical microscope [10], an instrument that selectively images small particles in a translucent medium having multiple scattering sources. It reduces the problem of background clutter by providing spatial selectivity of both the illuminating and backscattered waves. Our UWB pulsed adaptation achieves a range-gated microwave focus at potential tumor locations through the use of an electronically scanned antenna array of N elements. Here, an ultrawide-band antenna element located at a particular position on the surface of the breast is excited and the backscattered waveform is collected, digitized, and stored within the computer. Via electronic switching, this is repeated in sequence for the other elements in the array. As a postprocessing step, the set of N backscattered waveforms are then variably time-shifted to achieve coherent addition for a desired virtual focal point within the breast in a manner analogous to the signal processing performed for geophysical seismic prospecting [11]. Backscatter from the in-breast focal point adds coherently in this process, while returns from off-focus scatterers add incoherently and are thereby suppressed.

Manuscript received July 29, 1998; revised December 2, 1998. This work was supported in part by the Small Business Innovative Research Grant 1-R43-CA67598-D1A2 from the National Institute of Health and by internal funding from Interstitial, Inc. Computing resources were provided by Cray Research, Inc.

S. C. Hagness is with the Department of Electrical and Computer Engineering, University of Wisconsin-Madison, Madison, WI 53706 USA.

A. Taflove is with the Department of Electrical and Computer Engineering, McCormick School of Engineering and Applied Science, Northwestern University, Evanston, IL 60208 USA.

J. E. Bridges is with Interstitial, Inc., Park Ridge, IL 60068 USA.

Publisher Item Identifier S 0018-926X(99)04839-5.

0018–926X/99$10.00 © 1999 IEEE

The position of the focal point is scanned throughout the breast by adjusting the assumed distribution of time shifts of the stored backscatter waveforms.

The spatial selectivity of the pulsed confocal microwave technology addresses a central problem in applying electrical or microwave techniques to tumor detection: the heterogeneous nature of the breast. Published microwave backscatter methods [12], [13] that illuminate the breast with large unfocused beams suffer because returns from a tumor can be masked by clutter from adjacent breast regions. Matrix schemes using microwave or impedance measurements [14], [15] suffer because errors in the data can be amplified by the matrix-inversion process. Alternative matrix schemes are under development for microwave imaging of objects embedded in lossy media [16]. Our approach has no relation to matrix schemes or techniques involving passive thermography or active tomography [17]. Three wide-ranging U.S. patents for our technology were awarded recently [18]–[20]; additional U.S. patents are pending.

Previously, we reported extensive two-dimensional (2-D) finite-difference time-domain (FDTD) simulations of the operation of the pulsed confocal technology [21]–[24]. In this paper, we present the methodology and results from three-dimensional (3-D) FDTD modeling of key system aspects relating to the UWB antenna-element design, the propagation and scattering of the electromagnetic impulse radiated by this element within a simple model of the breast, and the polarization and spectral characteristics of the backscatter response of generic tumor shapes. The results reported here and in [21]–[24] indicate that a system realized with existing microwave equipment has sufficient sensitivity and dynamic range to detect small tumors less than 5 mm in diameter located within 5 cm of the skin surface.

II. Summary of Breast Tissue Dielectric Properties

Breast-tissue differentiation using the pulsed microwave confocal approach is based upon two fundamental physical properties.

1) The high-water content of malignant tumors causes them to have significantly larger microwave scattering cross sections than normal fatty breast tissues that have low-water content. The vascularization of malignant tumors further increases the scattering cross section.
2) Microwave attenuation in normal breast tissue is low enough (less than 4 dB/cm up to 10 GHz) to permit constructive addition of wide-bandwidth backscattered returns using broad-aperture confocal-imaging techniques.

Specifically, Gabriel *et al.* [25]–[27] reported that the relative dielectric permittivity, ϵ_r, and conductivity, σ, of high-water-content tissues such as muscle are about an order of magnitude greater than those found for low-water-content tissues such as fat. This contrast persists throughout the entire RF spectrum up through millimeter waves. Foster and Schepps [28], Rogers *et al.* [29], and Peloso *et al.* [30] reported that the dielectric properties of malignant tumors are almost the same as those found for normal high-water-content tissues such as muscle.

Joines *et al.* [31] and Chaudhary *et al.* [32] performed a large number of measurements up to 3 GHz of both normal and malignant human breast tissues. They found that the dielectric properties of normal breast tissues are similar to (but somewhat greater than) fat, while the properties of malignant breast tumors are similar to muscle. According to their measured data, the dielectric properties of normal breast tissue properties vary in an approximate $\pm 10\%$ range about $\epsilon_r = 9$ and $\sigma = 0.4$ S/m, whereas for malignant tumors, $\epsilon_r = 50$ and $\sigma = 7$ S/m. Extrapolation of these values to higher frequencies using either the Debye model or an empirical model [33] shows that normal breast tissue exhibits path losses of less than 4 dB/cm up to 10 GHz.

Swarup *et al.* [35] studied the onset of the high values of ϵ_r and σ in malignant tumors by measuring MCA1 fibrosarcoma mouse tumors at 7, 15, and 30 days after inception. No significant variation of ϵ_r and σ was seen with tumor age. While the larger tumors exhibited a necrotic interior, they showed little difference in ϵ_r and σ above 0.5 GHz.

Surowiec *et al.* [36] performed measurements of centimeter-size malignant human breast tumors and adjacent tissues and found an increase in ϵ_r and σ of the normal breast tissue near malignant tumors. This effect may be caused by infiltration or vascularization. It could enlarge the microwave scattering cross section and thereby aid in the confocal microwave detection of the tumor.

Campbell and Land [34] also measured the dielectric properties of breast tissues with tumors. However, their data are not in agreement with the work cited above. Such discrepancies most likely are due to their experimental protocol which: 1) did not consider possible vascularization surrounding the tumors and 2) introduced air gaps in the very small dielectric-sample test chamber.

Some benign tumors may also have a high-water content and could produce a backscatter response similar to that generated by malignant tumors. However, at present, there exists little reliable data regarding the dielectric properties of benign tumors. Characterizing and analyzing such benign tumors is an extensive subject by itself and will be considered in future papers. Here, we focus only on the dielectric properties of malignant tumors.

III. Ultralow Reverberation Antenna Design for Biological Sensing

Video pulse radars operated at the air–earth interface have been used to detect buried structures such as pipes, cables, and mines [37]. Versions of these radars were proposed as means to detect and possibly image internal biological tissues [38]. However, a problem arises in that small or weakly-scattering tissue structures adjacent to an impulsively excited antenna can be obscured by the reflections from the ends of the antenna. (Early-time reflection due to impedance mismatch between the source cable and the antenna is assumed to be fully decayed before the end reflections.) For the case of free-space radiation of ultrawide-band video pulses, resistively loaded conical, and bowtie antennas have been reported [39], [40] having end reflections 40–50 dB below the exciting pulse.

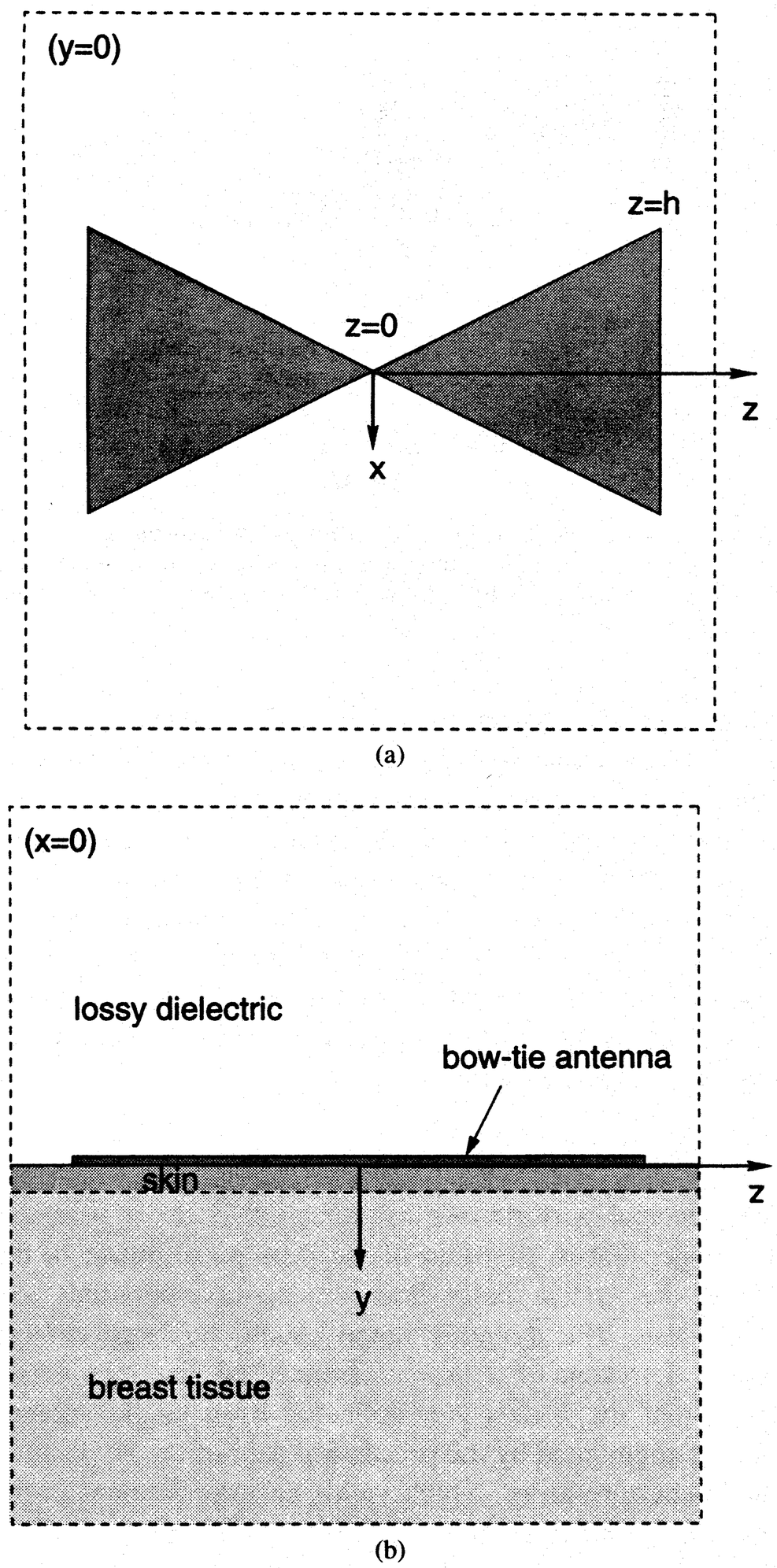

Fig. 1. Geometry of the bowtie antenna backed with a lossy dielectric slab, located at the surface of the breast tissue half-space (skin: $\epsilon_r = 36.0, \sigma = 4.0$ S/m, thickness = 1.0 mm; normal breast tissue: $\epsilon_r = 9.0, \sigma = 0.4$ S/m): (a) plan view and (b) side view.

As demonstrated in Section IV, this reflection level is too high for detecting tumors in the breast.

We recently reported the design of a wide-band bowtie antenna suitable for near-surface biological sensing [41]. The design procedure involved 3-D FDTD modeling [42], [43] in the manner of [39], [40], and [44]. In fact, the design was based upon a modification of the continuous resistive loading examined in [39], [40] in combination with the use of a zero dc Gaussian-pulse modulated carrier excitation and the location of the antenna at the interface of the biological tissue half-space. Here, we present the design of the antenna for use as an element in the pulsed microwave confocal array.

Fig. 1 shows the antenna configuration. A bowtie antenna with a flare length of $h = 4$ cm and a flare angle of 53° is located at the surface of the breast. The breast model is comprised of a 1-mm-thick layer of skin ($\epsilon_r = 36$ and $\sigma = 4.0$ S/m)[1] and a half-space of normal breast tissue ($\epsilon_r = 9$ and $\sigma = 0.4$ S/m). The antenna is comprised of a material that has the following conductivity:

$$\sigma(z) = \sigma_0 \cdot \frac{1 - z/h}{1 + (\sigma_0/\sigma_{1/2} - 2) \cdot (z/h)} \text{ S/m} \tag{1}$$

where z/h is the normalized axial distance along the bowtie, σ_0 is determined by the choice of the metal used at the feed point and $\sigma_{1/2}$ is chosen to give the desired level of suppression of the reflected pulse. As noted in [41], this taper is a modification of that used in [40]. Here, σ is a function of the axial distance z from the center of the bowtie, rather than a function of the radial distance. Also, $\sigma(z = 0) = \sigma_0$ in our design so that the conductivity at the center of the bowtie is large but finite. At the ends of the bowtie antenna ($z = \pm h$), the conductivity goes to zero. The antenna is embedded within a large block of lossy dielectric material that matches the dielectric parameters of normal breast tissue.

The excitation to the antenna is of the form

$$V(t) = V_0 \sin\left[2\pi f(t - t_0)\right] e^{-[(t-t_0)/\tau]^2} \text{ V} \tag{2}$$

where $f = 6$ GHz, $\tau = 0.133$ ns, and $t_0 = 4\tau$. This pulse has a temporal width of 0.22 ns (full width at half maximum—FWHM), an amplitude spectral width of 4 GHz (FWHM), and zero dc content. Although very wide-band, this excitation differs significantly from that used in [39] and [40]. Here, the excitation spectrum is a bandpass Gaussian function (centered about 6 GHz), which nulls out the low-frequency energy and minimizes the resulting exponential field decay in the surrounding lossy medium.

In the FDTD analysis, the slanted edges of the bowtie antenna are approximated using staircasing with a submillimeter spatial-grid resolution. The excitation is implemented as a 1-V, 50-Ω resistive voltage source at the antenna feedpoint [45]. The FDTD grid is terminated with a perfectly matched layer absorbing boundary condition [46].

Fig. 2(a) graphs the FDTD-computed exciting pulse as observed at the feed point. The magnetic field recorded in this simulation circulates about the z-directed voltage source and is, therefore, proportional to the induced current.

Fig. 2(b) graphs the FDTD computed-end reflections as observed at the feed point of the all-metal bowtie antenna. The end reflection is seen to be −63 dB relative to the exciting pulse. Evidently, the lossy nature of the skin provides a substantial amount of suppression of the end reflections. For example, in our previously reported work, which did not include the skin layer, the reflection from the ends of the all-metal antenna was seen to be −40 dB [41].

Fig. 2(c) graphs the FDTD computed-end reflections as observed at the feed point of the resistively loaded bowtie antenna for which $\sigma_0 = 3.27 \times 10^7$ S/m (the conductivity of a typical metal) and $\sigma_{1/2} = 1.0$ S/m (a sheet resistance of 1000

[1] Gabriel *et al.* [25]–[27] found that, for either wet or dry skin, $30 < \epsilon_r < 40$ and $1 < \sigma < 10$ S/m from 1–10 GHz.

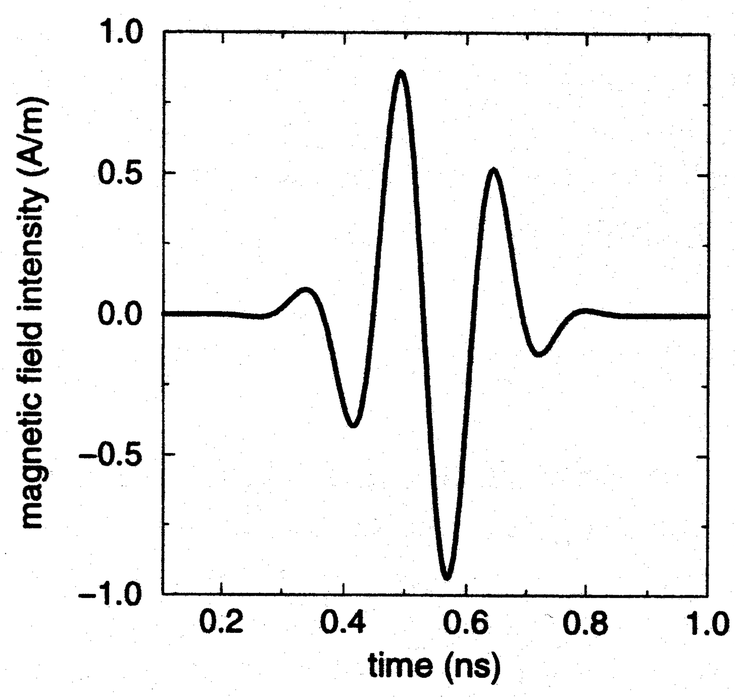

(a)

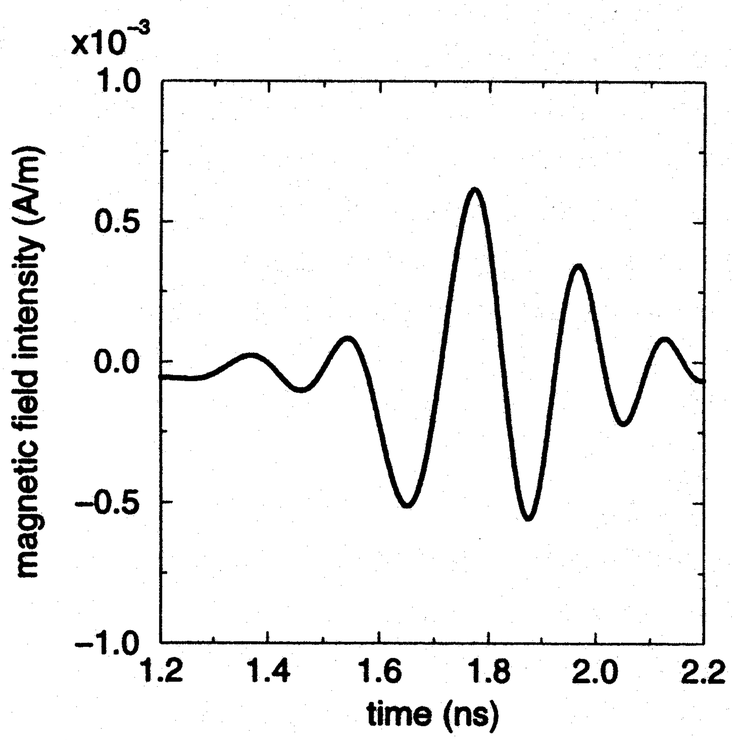

(b)

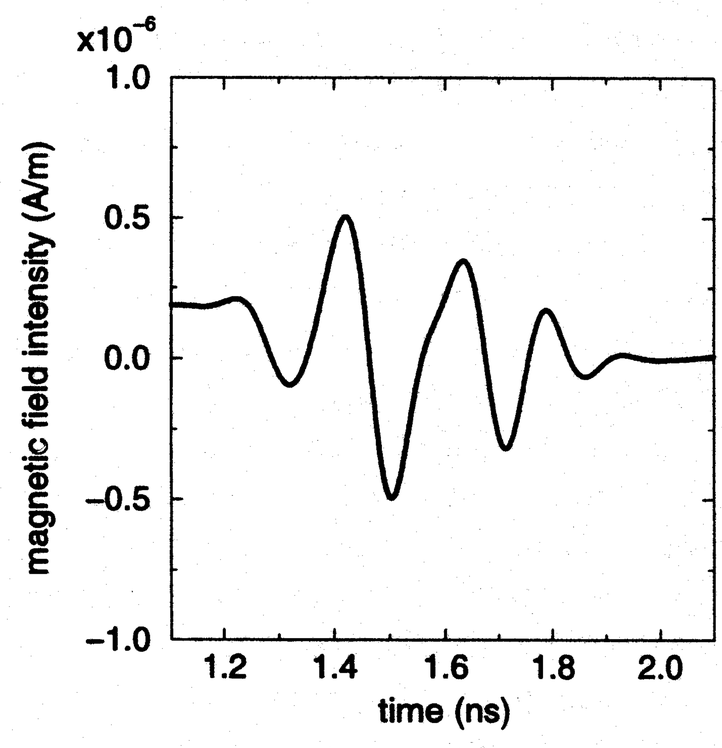

(c)

Fig. 2. Time-domain fields observed at the feed point of the bowtie antenna shown in Fig. 1. (a) Exciting pulse. (b) Pulse reflected from the ends of the all-metal antenna. (c) Pulse reflected from the ends of the resistively loaded antenna.

Ω, assuming an antenna thickness of 1 mm). The resistive loading together with the lossy nature of the biological tissue and the bandpass nature of the excitation drops the antenna reverberation to -125 dB relative to the exciting pulse. In comparison to Fig. 2(b), the resistive loading is seen to provide an additional 60 + dB of dynamic range beyond that which is

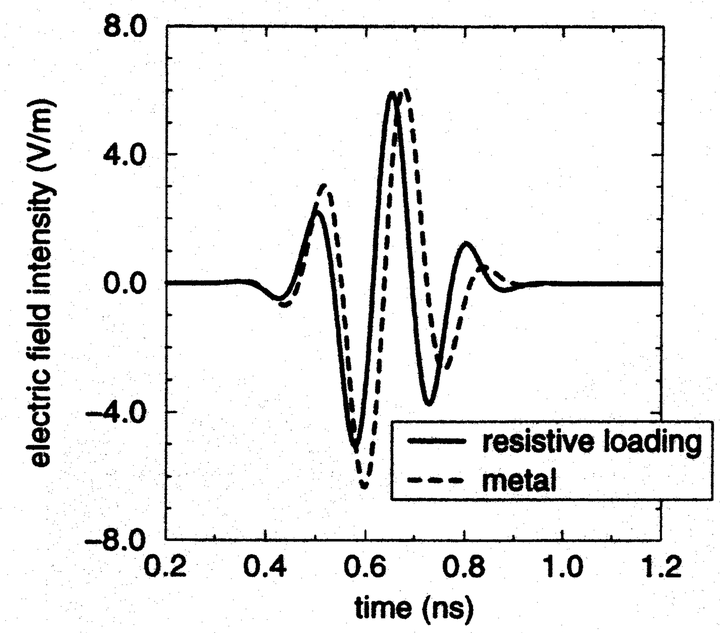

Fig. 3. Time-domain fields observed at a depth of 1.0 cm in the breast tissue half-space. The fields radiated by the resistively loaded bowtie antenna (solid line) are reduced in amplitude by 1 dB relative to the all-metal bowtie antenna (dotted line).

available with the all-metal version of the antenna in Fig. 1. Further, the resistive loading causes little loss of radiating efficiency for the electric fields penetrating the tissue half-space. Fig. 3 graphs the FDTD computed z-directed electric fields at a depth of 1 cm below the feed point. The pulse radiated by the resistively loaded antenna into the breast is reduced by only 1.0 dB relative to the all-metal antenna. As shown in Section IV, this ultralow reverberation antenna permits the sensing of tumors less than 5 mm in diameter at depths as great as 5.0 cm.

IV. Dynamic Range

The principal performance specification is the system dynamic range; that is, the ratio of the peak pulse power of the source to the system noise floor due to reverberations and thermal noise. The dynamic range should be large enough to permit detection of a tumor of specified size and depth. We note that the backscatter collected by a single antenna element is augmented by the processing gain of the N-position synthetic-aperture array, which yields an improvement in the signal-to-noise ratio of $10 \log N$ dB. Assuming $10 \leq N \leq 100$, the processing gain would range between 10–20 dB.

Using the resistively loaded bowtie antenna, we have performed benchmark simulations to estimate the dynamic range requirements of the microwave system. The 3-D FDTD model used for this study is similar to that shown in Fig. 1, except that here a spherical malignant tumor is embedded within the breast tissue half-space. The depth of a typical normal, nonlactating human breast is on the order of 5 cm [47]–[49]. This suggests that a flattened breast of a patient in supine position would span less than 5 cm between the skin surface and the rib cage. Further, almost 50% of all breast tumors occur in the quadrant near the underarm where the breast is less than about 2.5 cm deep [50]. Accordingly, we have based our computational models of the confocal microwave system on detecting tumors to depths of up to 5 cm with a typical depth of 3–4 cm.

To determine the dynamic range required to detect a tumor of a specific diameter and depth, the peak-to-peak amplitude of the backscattered response of the tumor is compared with the peak-to-peak amplitude of the exciting pulse. Fig. 4 graphs the

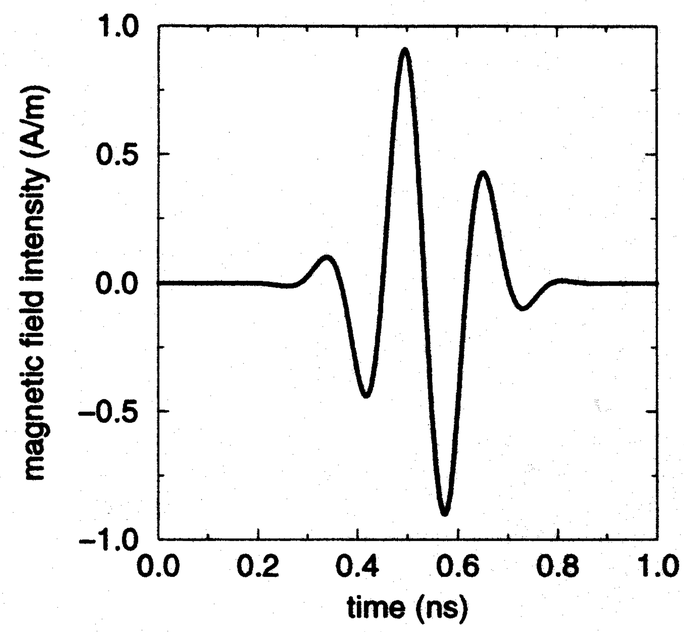

(a)

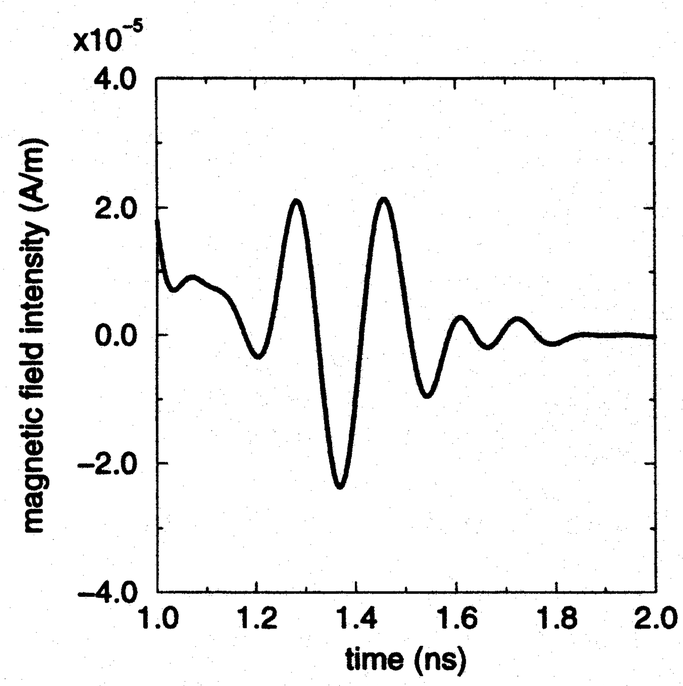

(b)

Fig. 4. Time-domain fields observed at the feed point of the bowtie antenna. A 0.5-cm-diameter spherical tumor is located in the breast tissue half-space at a depth of 4.0 cm directly below the feedpoint. (a) Exciting pulse. (b) Backscattered response of tumor.

FDTD-computed magnetic field circulating the feed point for the case of a 5.28-mm-diameter tumor located at a depth of 4.0 cm directly below the feed point. The backscatter from the tumor [Fig. 4(b)] observed in the 1.0-ns time window immediately following the excitation [Fig. 4(a)] is seen to be −92 dB relative to the exciting pulse. This simulation was performed for tumor diameters of 5.28, 3.52, and 1.76 mm at depths of 3.0, 4.0, and 5.0 cm. The backscatter response levels are tabulated in Table I and graphed in Fig. 5. As seen from the slope of the curves in Fig. 5(b), the peak power in the backscatter return drops approximately 9 dB per cm increase in the depth of the tumor.

The backscatter response for the "worst case" tumor studied here (diameter of 1.76 mm, depth of 5.0 cm) is seen to be −115 dB relative to the source power. We note that the −125-dB reverberation due to reflections from the ends of the resistively loaded bowtie antenna (reported in Section III) is sufficiently low enough to permit backscattered returns from this tumor to be sensed. Furthermore, we have observed a dynamic range in the order of 120 dB for the Hewlett-Packard HP8720D vector network analyzer when properly configured and programmed with processing times adequate for preclinical testing. This can be improved to 135 dB with minor modifications. Thus, given the discussion above, our optimized resistively loaded bowtie antenna in combination with commercial vector network analyzers yield more than adequate dynamic range for our tumor-detection system.

TABLE I
NORMALIZED BACKSCATTER DATA AS A FUNCTION OF THE TUMOR DIAMETER AND DEPTH

tumor depth	tumor diameter	tumor response
3.0 cm	5.28 mm	-83 dB
	3.52 mm	-88 dB
	1.76 mm	-96 dB
4.0 cm	5.28 mm	-92 dB
	3.52 mm	-97 dB
	1.76 mm	-106 dB
5.0 cm	5.28 mm	-101 dB
	3.52 mm	-106 dB
	1.76 mm	-115 dB

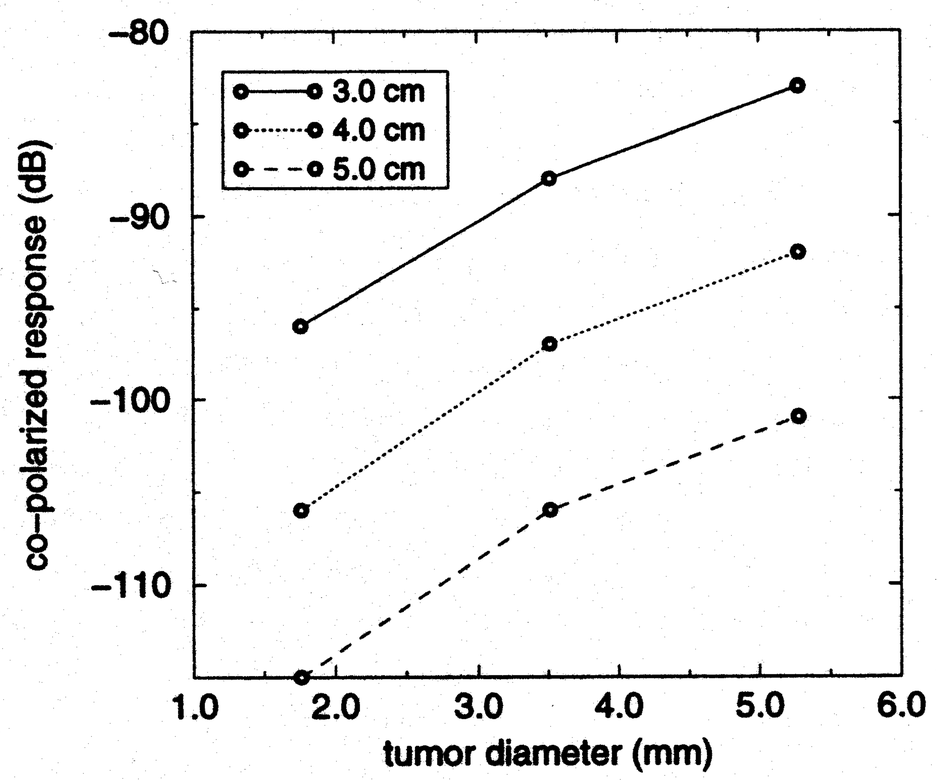

(a)

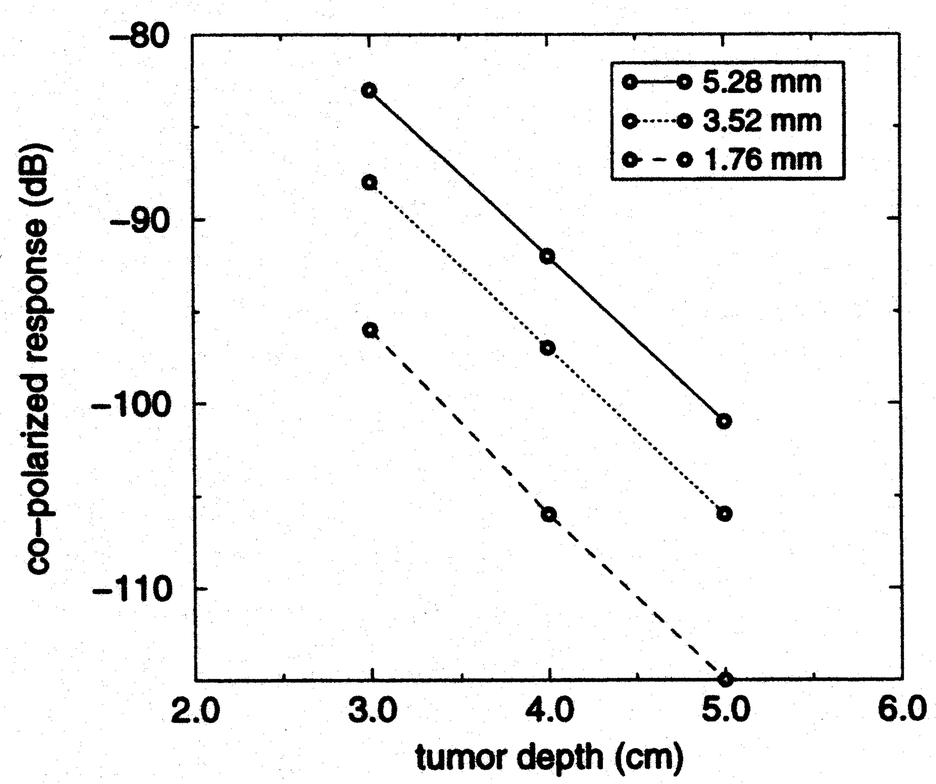

(b)

Fig. 5. Normalized backscatter data plotted as (a) a function of tumor diameter (constant depth) and (b) a function of tumor depth (constant diameter).

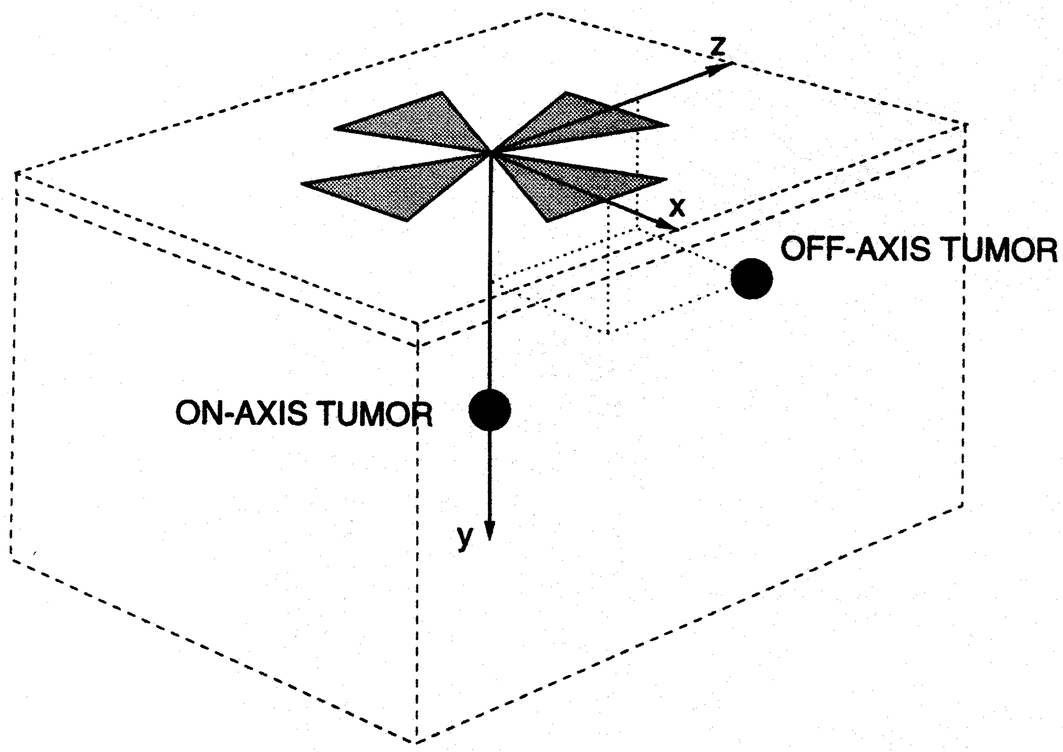

Fig. 6. Geometry of the perpendicular bowtie antenna elements forming a Maltese cross. Examples of axially symmetric and axially asymmetric tumors are illustrated.

V. Cross-Polarized Antenna Elements

By exciting one antenna of a pair of perpendicular antenna elements forming a Maltese cross and receiving on the other antenna, the cross-polarized backscattered return from a tumor can be obtained. Fig. 6 shows this antenna configuration. The cross-polarized backscatter of an axially symmetric tumor such as the spherical tumor positioned directly below the antenna feed point, labeled as an "on-axis" tumor in Fig. 6, is exactly zero. However, when the antenna pair is positioned such that the tumor is off the central perpendicular axis of the two antennas, as is the case of the "off-axis" tumor shown in Fig. 6, there is a nonzero cross-polarized component of the tumor backscatter. The cross-polarized component is nonzero for any axially asymmetric tumor. A second example of an axially asymmetric tumor is a cylindrical tumor located on the y axis, oriented at 45° with respect to the x and z axes.

One of the key advantages of using the Maltese cross configuration is that tumors adjacent to the planar chest wall can be detected. We illustrate this feature by repeating the 3-D simulation with a chest wall present in the model. The chest wall is modeled as a planar half-space beginning at a depth of 4.0 cm below the skin surface. The dielectric parameters for the chest wall are assumed to be those of muscle ($\epsilon_r = 50$ and $\sigma = 7$ S/m). A 6.4-mm-long 3.2-mm-diameter cylindrical tumor is located within the breast tissue model at a depth of 3.72 below the feed point along the y axis, oriented at 45° with respect to the crossed antennas. The distance between the tumor and the plane of the chest wall is only 0.8 mm.

Fig. 7 shows the FDTD-computed co- and cross-polarized waveforms for this model. The pulse excited by the transmitting antenna [shown in Fig. 7(a)] is a differentiated Gaussian with the following time dependence:

$$V(t) = V_0(t - t_0)\, e^{[(t-t_0)/\tau]^2} \text{ V} \tag{3}$$

where $\tau = 0.07$ ns, and $t_0 = 4\tau$. This pulse has a temporal width of 0.19 ns (FWHM), an amplitude spectral width of 5.2 GHz (FWHM), and zero dc content. We chose a different pulse shape here to verify that our proposed detection system

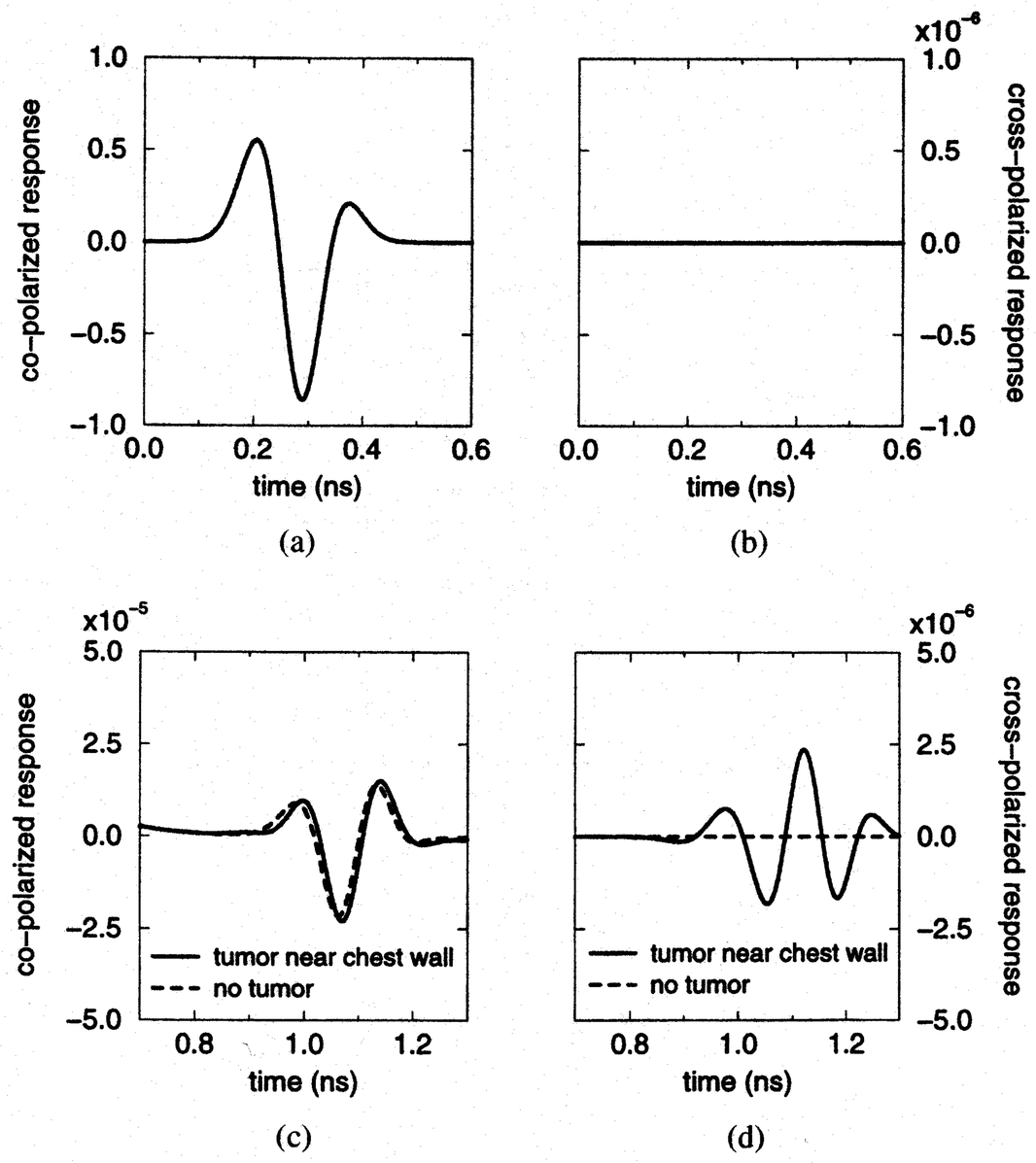

Fig. 7. Time-domain fields observed near the feedpoint of a perpendicularly bisecting pair of antennas located at the skin surface. A 6.4-mm-long 3.2-mm-diameter cylindrical tumor is located within the breast tissue at a depth of 3.72 cm below the feedpoint, oriented at 45° with respect to the crossed antennas. A planar chest wall is located at a depth of 4.0 cm. (a) Early-time copolarized response shows the exciting pulse. (b) Early-time cross-polarized response shows complete rejection of crosstalk. (c) Later-time copolarized response shows that the backscatter from the chest wall dominates. (d) Later-time cross-polarized response shows a rejection of the chest wall backscatter and a clear observation of the tumor backscatter.

is robust relative to the precise shape of the exciting pulse. Fig. 7(b) graphs the cross-polarized response observed during the same time window, showing that the cross-polarized receiving antenna rejects crosstalk from the transmitting antenna. The dotted-line curves shown in Fig. 7(c) and (d) are obtained from a simulation of a tumor-free breast with the chest wall included. The simulation is repeated for the model with the tumor present; those results are graphed as solid lines. As shown in Fig. 7(c), the tumor near the chest wall cannot be detected by observing the copolarized fields since the backscatter from the chest wall dominates the copolarized response. However, as illustrated in Fig. 7(d), cross-polarized sensing rejects unwanted backscatter from the chest wall, permitting the detection of the tumor adjacent to the chest wall.

VI. Spectral Content of the Backscatter Response

Malignant tumors are typically asymmetrical and spiculated, while most benign masses are well-circumscribed and compact [51]. Our 3-D FDTD simulations have indicated the possibility of distinguishing between benign and malignant tumors (regardless of the dielectric properties of benign tumors) by exploiting the morphology-dependent spectral and polarization characteristics of their microwave backscatter response. Fig. 8 graphs the FDTD-computed backscatter spectral char-

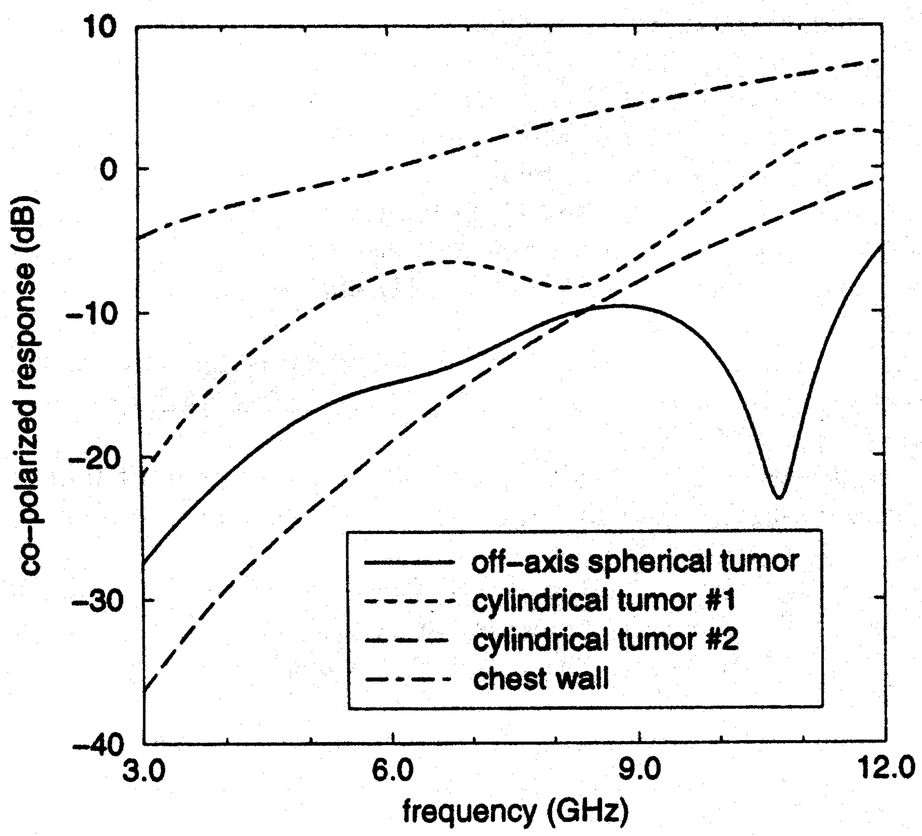

(a)

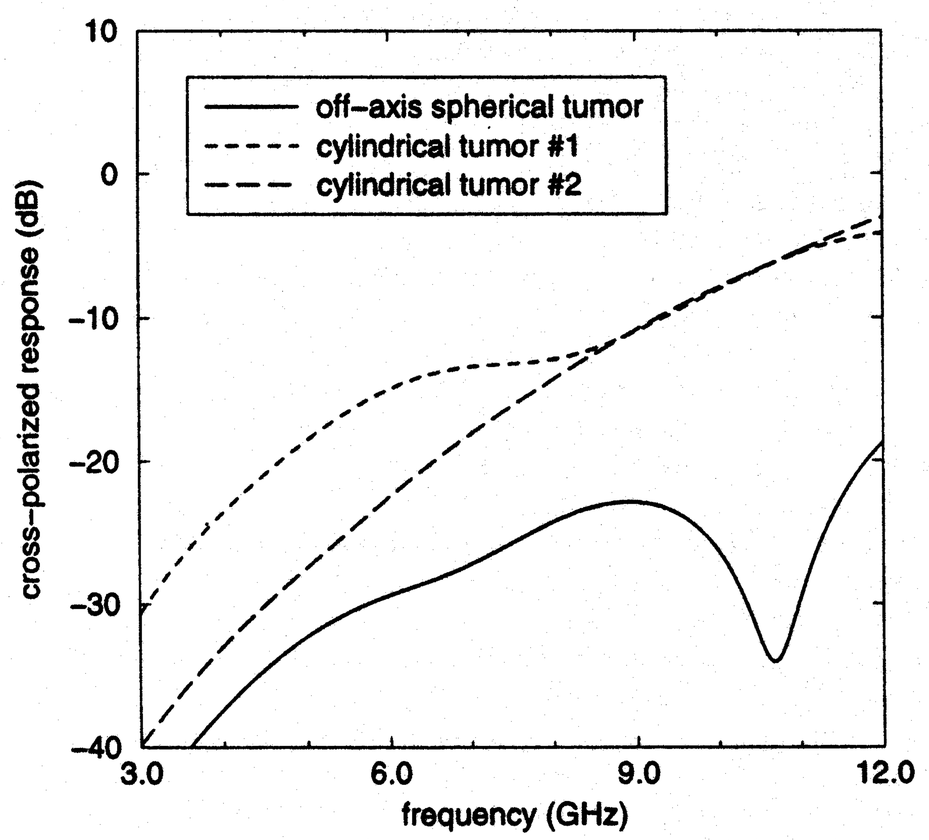

(b)

Fig. 8. Backscatter spectra for the crossed-dipole antenna system. (a) Copolarized response. (b) Cross-polarized response. All power levels have been normalized with respect to the incident spectrum and are shown relative to the copolarized response of the chest well at 6 GHz.

acteristics of three tumor shapes: a 0.5-cm-diameter off-axis spherical tumor (solid line); an asymmetrically oriented on-axis cylindrical tumor with a diameter of 0.32 cm and a length of 0.64 cm (#1, dotted line); and a second cylindrical tumor with a diameter of 0.08 cm and a length of 0.72 cm (#2, dashed line). In each of the three simulations, the tumor is located at a distance of 3 cm from the antenna feed point. For reference, the spectral content of the chest wall backscatter is also graphed (dot-dashed line). All response levels are plotted relative to the copolarized response of the chest wall at 6 GHz [the 0-dB point in Fig. 8(a)].

In Fig. 8(a), the copolarized backscatter response of each tumor is seen to be well below the response of the chest wall, further illustrating the need to observe the cross-polarized return (for which the backscatter from the idealized planar chest wall is nonexistent). The spectral characteristic of the spherical tumor is markedly different from that of a planar or less-compact scatterer. Specifically, the spherical tumor can be distinguished from the cylindrical tumors by a deep null in its backscatter spectrum. As shown in Fig. 8(b), the cross-polarized response of each tumor retains the spectral characteristics of the copolarized response. For each tumor, the overall cross-polarized return is, on average, 10 dB below that of the copolarized return.

VII. Summary and Conclusions

This paper presented the methodology and initial results of 3-D FDTD simulations of a resistively loaded bowtie antenna planned for use as an element of an UWB microwave sensor array to detect and image early-stage malignant breast tumors. Key aspects relating to the antenna-element design were discussed. These included: 1) optimizing the resistive loading for minimum end reflections; 2) evaluating the copolarized backscattering of the electromagnetic pulse radiated by this element by idealized spherical tumors of various sizes at several depths within the homogeneous breast; and 3) evaluating the polarization and frequency-response characteristics of generic tumor shapes.

The 3-D FDTD simulations show that the UWB end reflections for the bowtie element can be reduced to −125 dB with the proper resistive loading. Fortunately, this optimal loading reduces the desired radiation by only about 1 dB. For this optimized element, the copolarized backscatter responses of spherical tumors of diameters 1.7–5.3 mm embedded within the breast at depths of 3–5 cm are in the range of −80 to −115 dB. For a perpendicular pair of antenna elements, the cross-polarized backscatter responses for various generic tumor shapes are about 10 dB below the corresponding copolarized responses.

From these simulations, we conclude that the radiating bandwidth and backscatter dynamic-range characteristics of an optimized resistively loaded bowtie antenna (and its associated Maltese cross) are sufficient to permit the detection of many early-stage malignant breast tumors when used in conjunction with existing commercial microwave instruments. In fact, we have recently constructed a laboratory prototype sensor element that uses the Maltese-cross antenna in conjunction with a simple breast phantom. Measured data obtained with this system are consistent with our simulation results. A description of these experiments is beyond the scope of this paper and may be provided in a subsequent paper. We are currently conducting large-scale FDTD simulations of an array of Maltese-cross elements in the context of more realistic anatomically based models of the breast. Using these simulations as a design tool, we are constructing a sensor system for preclinical experimentation.

Acknowledgment

The authors would like to thank Prof. A. Sahakian, Northwestern University, Evanston, IL, for technical guidance. They would also like to thank Prof. M. Griem, University of Chicago, Dr. J. Aarsvold, Atlanta Veterans Administration

Medical Center, and Dr. F. Kelcz, University of Wisconsin-Madison, who served as medical consultants.

REFERENCES

[1] J. R. Harris, M. E. Lippman, U. Veronesi, and W. Willett, "Medical progress: Breast cancer," *New Eng. J. Med.*, vol. 327, no. 5, pp. 319–328, 1992.

[2] C. Boetes, R. D. M. Mus, R. Holland, J. O. Barentsz, S. P. Strijk, T. Wobbes, J. H. C. L. Hendriks, and S. H. J. Ruys, "Breast tumors: Comparative accuracy of MR imaging relative to mammography and U.S. for demonstrating extent," *Radiol.*, vol. 197, no. 3, pp. 743–747, 1995.

[3] F. M. Hall, J. M. Storella, D. Z. Silverstone, and G. Wyshak, "Nonpalpable breast-lesions: Recommendation for biopsy based on suspicion of carcinoma at mammography," *Radiol.*, vol. 167, no. 2, pp. 353–358, 1988.

[4] J. G. Elmore, M. B. Barton, V. M. Moceri, S. Polk, P. J. Arena, and S. W. Fletcher, "Ten-year risk of false positive screening mammograms and clinical breast examinations," *New Eng. J. Med.*, vol. 338, no. 16, pp. 1089–1096, 1998.

[5] E. D. Staren and T. P. O'Neill, "Breast ultrasound," *Surgical Clinic North Amer.*, vol. 78, no. 2, pp. 219–235, 1998.

[6] C. Maestro, F. Cazenave, P. Y. Marcy, J. N. Bruneton, C. Chauvel, and A. Bleuse, "Systematic ultrasonography in asymptomatic dense breasts," *Eur. J. Radiol.*, vol. 26, no. 3, pp. 254–256, 1998.

[7] G. M. Kacl, P.-F. Liu, J. F. Debatin, E. Garzoli, R. F. Caduff, and G. P. Krestin, "Detection of breast cancer with conventional mammography and contrast-enhanced MR imaging," *Eur. Radiol.*, vol. 8, no. 2, pp. 194–200, 1998.

[8] P. Viehweg, I. Paprosch, M. Strassinopoulou, and S. H. Heywang-Köbrunner, "Contrast-enhanced magnetic resonance imaging of the breast: Interpretation guidelines," *Topical Magn. Resonance Imaging*, vol. 9, no. 1, pp. 17–43, 1998.

[9] ANSI/IEEE C95.1-1992, *American National Standard—Safety Levels with Respect to Human Exposure to Radio Frequency Electromagnetic Fields, 3 kHz to 300 GHz.* New York: IEEE Press, 1992.

[10] J. P. Pawley, *Handbook of Biological Confocal Microscopy*, 2nd ed. New York: Plenum, 1995.

[11] P. Kearey and M. Brooks, "Seismic reflection surveying," in *Geosci. Texts, Vol. 4: An Introduction to Geophysical Exploration.* Boston, MA: Blackwell Sci., 1984, ch. 4.

[12] A. W. Preece, H. Johnson, F. L. Green, and M. P. Robinson, "Dielectric imaging for localization and detection of breast tumors," in *IEEE MTT Int. Microwave Symp. Dig.*, 1993, pp. 1145–1146.

[13] R. E. Sepponen, "Medical diagnostic microwave scanning apparatus," U.S. Patent 4 641 659, Feb. 10, 1987.

[14] W. Guo and T. Guo, "Quantitative dielectric imaging system," U.S. Patent 5 363 050, Nov. 8, 1994.

[15] B. D. Sollish, E. H. Frie, E. Hammerman, S. B. Lang, and M. Moshitsky, "Microprocessor-assisted screening technique," *Israel J. Med. Sci.*, vol. 17, pp. 859–864, 1981.

[16] W. C. Chew, "Imaging and inverse problems in electromagnetics," in *Advances in Computational Electrodynamics: The Finite-Difference Time-Domain Method*, A. Taflove, Ed. Boston, MA: Artech House, 1998, ch. 12.

[17] L. E. Larsen and J. H. Jacobi, Eds., *Medical Applications of Microwave Imaging.* New York: IEEE Press, 1986.

[18] J. E. Bridges, "Non-invasive system for breast cancer detection," U.S. Patent 5 704 355, Jan. 6, 1998.

[19] ——, "Breast cancer detection, imaging, and screening by electromagnetic millimeter waves," U.S. Patent 5 807 257, Sept. 15, 1998.

[20] ——, "Microwave method and system to detect and locate cancer in heterogeneous tissues," U.S. Patent 5 829 437, Nov. 3, 1998.

[21] S. C. Hagness, A. Taflove, and J. E. Bridges, "FDTD analysis of a pulsed microwave confocal system for breast cancer detection," in *Proc. Int. Conf. IEEE Eng. Med. Biol. Soc.*, Chicago, IL, Oct. 1997, pp. 2506–2508.

[22] ——, "FDTD modeling of a coherent-addition antenna array for early-stage detection of breast cancer," in *IEEE Antennas Propagat. Soc. Int. Symp.*, Atlanta, GA, June 1998, vol. 2, pp. 1220–1223.

[23] M. Popovíc, S. C. Hagness, A. Taflove, and J. E. Bridges, "2-D study of fixed-focus elliptical reflector system for breast cancer detection: Frequency window for optimum operation," in *IEEE Antennas Propagat. Soc. Int. Symp.*, Atlanta, GA, June 1998, vol. 4, pp. 1992–1995.

[24] S. C. Hagness, A. Taflove, and J. E. Bridges, "Two-dimensional FDTD analysis of a pulsed microwave confocal system for breast cancer detection: Fixed-focus and antenna-array sensors," *IEEE Trans. Biomed. Eng.*, vol. 45, pp. 1470–1479, Dec. 1998.

[25] C. Gabriel, S. Gabriel, and E. Corthout, "The dielectric properties of biological tissues—I: Literature survey," *Phys. Med. Biol.*, vol. 41, no. 11, pp. 2231–2249, Nov. 1996.

[26] S. Gabriel, R. W. Lau, and C. Gabriel, "The dielectric properties of biological tissues—II: Measurements on the frequency range 10 Hz to 20 GHz," *Phys. Med. Biol.*, vol. 41, no. 11, pp. 2251–2269, Nov. 1996.

[27] ——, "The dielectric properties of biological tissues—III: Parametric models for the dielectric spectrum of tissues," *Phys. Med. Biol.*, vol. 41, no. 11, pp. 2271–2293, Nov. 1996.

[28] K. R. Foster and J. L. Schepps, "Dielectric properties of tumor and normal tissue at radio through microwave frequency," *J. Microwave Power*, vol. 16, pp. 107–119, 1981.

[29] J. A. Rogers, R. J. Shepard, E. H. Grant, N. M. Bleehen, and D. J. Honess, "The dielectric properties of normal and tumor mouse tissue between 50 MHz and 10 GHz," *British J. Radiol.*, vol. 56, pp. 335–338, 1983.

[30] R. Peloso, D. Tuma, and R. K. Jain, "Dielectric properties of solid tumors during normothermia and hyperthermia," *IEEE Trans. Biomed. Eng.*, vol. 31, pp. 725–728, 1984.

[31] W. T. Joines, Y. Z. Dhenxing, and R. L. Jirtle, "The measured electrical properties of normal and malignant human tissues from 50 to 900 MHz," *Med. Phys.*, vol. 21, pp. 547–550, Apr. 1994.

[32] S. S. Chaudhary, R. K. Mishra, A. Swarup, and J. M. Thomas, "Dielectric properties of normal and malignant human breast tissues at radiowave and microwave frequencies," *Indian J. Biochem. Biophys.*, vol. 21, pp. 76–79, Feb. 1984.

[33] K. R. Foster and H. P. Schwan, "Dielectric properties of tissues and biological materials: A critical review," *Critical Rev. Biomed. Eng.*, vol. 17, pp. 25–104, 1989.

[34] A. M. Campbell and D. V. Land, "Dielectric properties of female human breast tissues measured *in vitro* at 3.2 GHz," *Phys. Med. Biol.*, vol. 37, no. 1, pp. 193–210, 1992.

[35] A. S. Swarup, S. S. Stuchly, and A. Surowiec, "Dielectric properties of mouse MCA1 fibrosarcoma at different stages of development," *Bioelectromagn.*, vol. 12, pp. 1–8, 1991.

[36] A. J. Surowiec, S. S. Stuchly, J. R. Barr, and A. Swarup, "Dielectric properties of breast carcinoma and the surrounding tissues," *IEEE Trans. Biomed. Eng.*, vol. 35, pp. 257–263, Apr. 1988.

[37] G. A. Burrell and L. Peters, Jr., "Pulse propagation in lossy media using the low-frequency window for video pulse radar application," *Proc. IEEE*, vol. 67, pp. 981–990, July 1979.

[38] J. D. Young and L. Peters, Jr., "Examination of video pulse radar systems as potential biological exploratory tools," in *Medical Applications of Microwave Imaging*, L. E. Larsen, and J. H. Jacobi, Eds. New York: IEEE Press, 1986, pp. 82–105.

[39] J. G. Maloney and G. S. Smith, "Optimization of a conical antenna for pulse radiation: An efficient design using resistive loading," *IEEE Trans. Antennas Propagat.*, vol. 41, pp. 940–947, July 1993.

[40] K. L. Shlager, G. S. Smith, and J. G. Maloney, "Optimization of bow-tie antennas for pulse radiation," *IEEE Trans. Antennas Propagat.*, vol. 42, pp. 975–982, July 1994.

[41] S. C. Hagness, A. Taflove, and J. E. Bridges, "Wideband ultralow reverberation antenna for biological sensing," *Electron. Lett.*, vol. 33, no. 19, pp. 1594–1595, 1997.

[42] K. S. Kunz and R. J. Luebbers, *The Finite Difference Time Domain Method for Electromagnetics.* Boca Raton, FL: CRC, 1993.

[43] A. Taflove, *Computational Electrodynamics: The Finite-Difference Time-Domain Method.* Boston, MA: Artech House, 1995.

[44] J. M. Bourgeois and G. S. Smith, "A fully three-dimensional simulation of a ground-penetrating radar: FDTD theory compared with experiment," *IEEE Trans. Geosci. Remote Sensing*, vol. 34, pp. 36–44, Jan. 1996.

[45] M. Piket-May, A. Taflove, and J. Baron, "FD-TD modeling of digital signal propagation in 3-D circuits with passive and active loads," *IEEE Trans. Microwave Theory Tech.*, vol. 42, pp. 1514–1523, Aug. 1994.

[46] J.-P. Berenger, "A perfectly matched layer for the absorption of electromagnetics waves," *J. Comput. Phys.*, vol. 114, pp. 185–200, Oct. 1994.

[47] H. Gray, *Anatomy of the Human Body*, C. M. Goss, Ed. Philadelphia, PA: Lea Febiger, 1949.

[48] X. Wu, G. T. Barnes, and D. M. Tucker, "Spectral dependence of glandular tissue dose in screen-film mammography," *Radiol.*, vol. 179, no. 1, pp. 143–148, Apr. 1991.

[49] M. Rosenstein, L. W. Andersen, and G. Warner, "Handbook of glandular tissue doses in mammography," HHS (FDA) Publication No. 858 239, U.S. Govt. Printing Office, Washington, DC, 1985.
[50] W. H. Parsons, *Cancer of the Breast.* Springfield, IL: Charles Thomas, 1959.
[51] R. M. Rangayyan, N. M. El-Faramawy, J. E. L. Desautels, and O. A. Alim, "Measures of acutance and shape for classification of breast tumors," *IEEE Trans. Med. Imaging,* vol. 16, pp. 799–810, Dec. 1997.

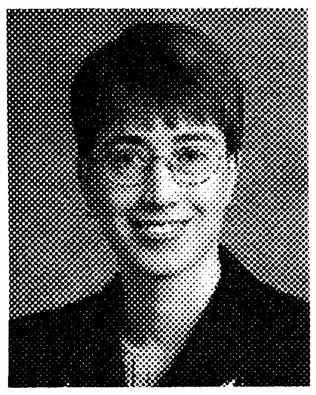

Susan C. Hagness (S'91–M'98) received the B.S. (highest honors) and Ph.D. degrees, both in electrical engineering, from Northwestern University, Evanston, IL, in 1993 and 1998, respectively.

She joined the Department of Electrical and Computer Engineering at the University of Wisconsin-Madison as an Assistant Professor in 1998. Her current research interests include computational electrodynamics, bioelectromagnetics, microwave imaging, antennas for diagnostic electromagnetic exposure systems, and very large scale integration (VLSI) photonics. She has published more than 30 refereed journal and conference papers.

Dr. Hagness was the recipient of the Eta Kappa Nu Norman R. Carson Award as the Outstanding Junior Electrical Engineering Student in the U.S. in 1992. In 1993, she received a National Science Foundation Graduate Fellowship and was named a Tau Beta Pi Spencer Fellow. She was awarded a Northwestern University Cabell Dissertation Year Fellowship in 1997 and the Department of Electrical and Computer Engineering Best Dissertation Award in 1998. She received the Student Paper Competition Third Prize Award at the 1998 IEEE AP-S International Symposium and URSI Radio Science Meeting. She is the recipient of the 1999 URSI Young Scientist Award. She is a member of Tau Beta Pi, Eta Kappa Nu, the Optical Society of America, the Bioelectromagnetics Society, the American Society for Engineering Education, and the Applied Computational Electromagnetics Society.

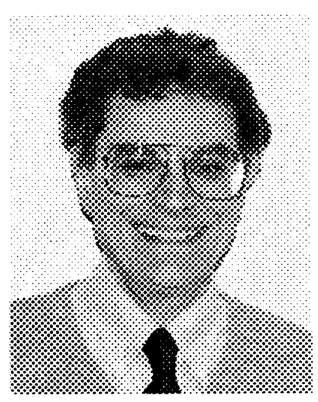

Allen Taflove (M'75–SM'84–F'90) received the B.S., M.S., and Ph.D. degrees in electrical engineering from Northwestern University, Evanston, IL, in 1971, 1972, and 1975, respectively.

After nine years as a Research Engineer at IIT Research Institute, Chicago, IL, he joined the faculty at Northwestern University and is currently a Professor in the Department of Electrical and Computer Engineering in that university. He has pioneered basic theoretical approaches and engineering applications of finite-difference time-domain computational electromagnetics. In 1990 and 1991 he was a Distinguished National Lecturer for the IEEE Antennas and Propagation Society (AP-S). He authored *Computational Electrodynamics: The Finite-Difference Time-Domain Method* (Norwood, MA: Artech House, 1995) and edited *Advances in Computational Electrodynamics: The Finite-Difference Time-Domain Method* (Norwood, MA: Artech House, 1998). He holds 11 U.S. patents. His current research interests include finite-difference time-domain simulations of microwave detection and imaging systems for early-stage breast cancer, diffraction by building structures in wireless microcells, and particle-beam propagation in complex accelerator cavities.

Dr. Taflove was Chairperson of the Technical Program of the IEEE AP-S International Symposium, Chicago, IL, in 1992. In 1990 he was named an IEEE Fellow. He is a Member of IEEE COMAR, Eta Kappa Nu, Tau Beta Pi, Sigma Xi, URSI Commissions B, D, and K, and the Electromagnetics Academy. His biographical listings include *Who's Who in Engineering*, *Who's Who in America*, *Who's Who in Science and Engineering*, and *Who's Who in American Education*.

Jack E. Bridges (A'50–M'55–SM'56–F'74–LF'91) received the B.S. and M.S. degrees in electrical engineering from the University of Colorado, Boulder, in 1945 and 1947, respectively.

Prior to 1961, he was employed by Andrew Corp., Zenith Radio, and Warwick Manufacturing, all in Chicago, IL. From 1961 to 1992 he was with IIT Research Institute, Chicago, IL, where he attained the rank of Senior Science Advisor and initiated new interdisciplinary technologies, including an electrical method to stimulate flow rates from oil wells and an RF low-temperature method to sterilize medical wastes. In 1993 he founded Interstitial, Inc., Park Ridge, IL, to develop novel technologies in the energy and biomedical fields. He is the author of more than 100 journal articles or presentations and he currently holds 64 U.S. patents.

Mr. Bridges was the recipient of the 1983 Distinguished Engineering Alumnus Award from the University of Colorado, the 1981 Power Engineering Society Best Paper Award for "Biological Effects of ELF Electric Fields," and the 1956 Browder J. Thompson Best Paper Award for "Detection of Television Signals in Thermal Noise." He is a member of Eta Kappa Nu, Tau Beta Pi, Sigma Xi, the Bioelectromagnetics Society, and the American Association of Physicists in Medicine.